Fast Force Clamp in Optical Tweezers: A Tool to Study the Kinetics of Molecular Reactions

Pasquale Bianco, Lorenzo Bongini, Luca Melli, Giulia Falorsi, Luca Salvi, Dan Cojoc and Vincenzo Lombardi

Abstract A dual-laser optical tweezers has been developed to study the mechanics of motor proteins or DNA filaments. A bead attached to one end of the specimen is trapped in the confocal point of the two lasers, while the other end is connected to a three-dimensional piezo-stage. The instrument can be operated under computer control either as a length clamp, applying length steps or ramps, or as a force clamp, applying abrupt changes in load of fixed magnitude and direction. The dynamic range of the instrument (0.5–75,000 nm in length and 0.5–200 pN in force) and the speed of the force feedback permit recording the kinetics of molecular and intermolecular phenomena such as the overstretching transition in double-stranded DNA (ds-DNA) or the generation of force and shortening by an ensemble of myosin motors pulling on an actin filament. We demonstrate the performance of the system

P. Bianco · L. Bongini · L. Melli · G. Falorsi · L. Salvi · V. Lombardi (✉)
Laboratory of Physiology, Department of Biology, University of Florence, Florence, Italy
e-mail: vincenzo.lombardi@unifi.it

P. Bianco
e-mail: pasquale.bianco@unifi.it

L. Bongini
e-mail: lnzbng@gmail.com

L. Melli
e-mail: luca.melli@unifi.it

G. Falorsi
e-mail: giuliafalorsi@gmail.com

L. Salvi
e-mail: luca.salvi1@stud.unifi.it

D. Cojoc
IOM—National Research Council, Trieste, Italy
e-mail: cojoc@iom.cnr.it

F. Benfenati et al. (eds.), *Novel Approaches for Single Molecule Activation and Detection*, Advances in Atom and Single Molecule Machines,
DOI: 10.1007/978-3-662-43367-6_7,

in recording for the first time the transient kinetics of the ds-DNA overstretching transition, which allows the determination of the underlying reaction parameters, such as rate constants and distance to the transitions state.

1 Single-Molecule Mechanics with Optical Tweezers

Optical traps (or tweezers) are an efficient method for studying the properties of biological systems such as motor proteins [18, 25, 37], nucleic acid structures [24, 34], and processive enzymes [28, 48], which work in the nanometer-piconewton scale. The method allows recording molecular or intermolecular events one at a time, which is otherwise impossible from molecule ensemble experiments in cell or tissue. In single-molecule mechanical experiments, the light from a focused laser beam is used to trap a microscopic dielectric bead (made of silica or polystyrene) in a three-dimensional potential well centered near the focal point [3]. For a few hundreds of nanometers displacement from the equilibrium position, the trapping potential is harmonic, the restoring force varies linearly with the displacement, and the optical trap can be approximated to a linear spring. The spring constant, or stiffness, depends on the steepness of the optical gradient, i.e., how tightly the laser is focused and the laser power. In addition to the gradient force, there is a scattering force, due to the reflection on the bead surface, directed along the beam direction, which results in a shift of the equilibrium trapping position slightly past the focus. The high intensity of the trapping laser near the focus produces local heating, which is minimized using transparent dielectric beads and laser power not larger than 100 mW. To minimize photodamage of the biological specimen, laser wavelengths in the near infrared (800–1,100 nm) are preferred. With a laser power of 100 mW, the maximum force attained before exiting the linear region is around 50 pN and force resolution is approximately 0.1 pN.

The properties of the biological system under study are investigated by attaching the molecules of interest to the microscopic bead to bring it into contact with a fixed partner and measure the force and the displacement generated by the interaction. This type of assay has been first applied to the mechanical characterization of optically trapped motor protein kinesin moving along fixed microtubules (Fig. 1a; [6, 38, 42]). Processive motors, such as RNA polymerase, kinesin, and myosin V, spend a large part of the ATPase cycle time attached to their track, undergoing several steps from the start of the interaction, so that it is easy to measure the movement produced by a single motor and its speed in relation to the load carried by the motor. Muscle myosin II is not a processive motor and spends only a small fraction of the ATPase cycle time attached to the actin filament. Motor systems based on myosin II are organized in arrays (as it occurs for the myosin filament in the muscle sarcomere), and by this collective organization, they cooperatively maintain continuous interactions with the actin filament, producing steady force and filament sliding at high velocity. However, in single-molecule experiments, the

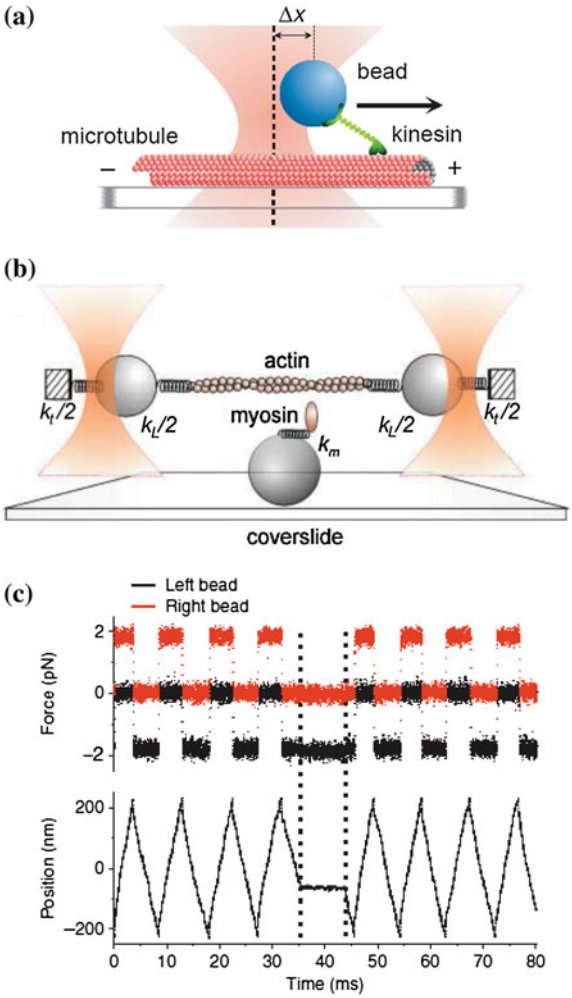

Fig. 1 **a** Motility assay used to record the activity of the processive motor kinesin (*green*) stepping along a microtubule (*red*). The distance between bead (*blue*) and trap (*pink*), Δx, was fixed at 175 nm, corresponding to a load of 6.5 pN, by moving the trap with AOD during the stepping. From Visscher et al. [42]. **b** Three-bead assay (*TBA*) to record the interaction of a myosin II motor with an actin filament. Both traps are static, and the interaction is recorded by the reduction of noise in the bead position due to the increase in stiffness of the system for the addition in parallel to the link stiffness (k_L) and trap stiffness (k_t) of the myosin stiffness (k_m). Modified from Capitanio et al. [10]. **c** Records of force on the left and the right beads (*top*) and position of one trap (*bottom*) in a TBA with fast force clamp. The force command that drives the AODs is switched periodically between positive and negative to keep the dumbbell within a confined spatial interval (±200 nm). The dumbbell stops when a myosin motor binds to the actin filament (between the *dotted lines*). From Capitanio et al. [11]

fast intermittent interactions of myosin II with actin cannot be resolved with the same trapping technique applied to processive motors. This limitation is overcame in the three-bead assay (TBA) configuration, in which the laser is split in two to trap the two ends of an actin filament which are manipulated by means of Acousto-Optic Deflectors (AOD) to bring and keep the filament into contact with a myosin motor attached to a third fixed bead [18]. However, also the TBA proved to be inadequate to measure the force and the load dependence of the movement generated by one myosin motor because the rise of force during a single myosin–actin interaction is largely affected by the low stiffness of attachments of the actin filament to the beads (k_L in Fig. 1b; see also Veigel et al. [41]). The system has been recently implemented with the introduction of the force clamp mode, which fixes the load on the bead and eliminates the change in length of the elastic components of the systems. This enables the control of the experimental conditions (isometric/isotonic) under which the motor works. In this ingenious implementation of the TBA [11], the force signal (determined by the position of each of the two actin attached beads) is the feedback signal that drives the two AOD in the laser path, so that the actin filament moves at the velocity necessary to generate the viscous force equal to the command force. When the myosin attaches to the actin filament, the filament stops moving as the force is now exerted by the myosin (Fig. 1c). The analysis of filament velocity reveals the duration of actin–myosin interactions and the associated length step. The system allows the mechanics of the event to be resolved within the first millisecond following the attachment. However, the concentration of ATP is kept at least 40 times lower than the physiological value to increase the lifetime of the events and make them detectable, and this in turns limits the power of the method for the determination of the load-dependent kinetics of the myosin–actin interaction.

Steady force and shortening in muscle are provided by cyclic actin attachment/detachment of myosin II motors working in parallel in the half-sarcomere. The collective nature of this motor can be studied at the nanometer scale in a synthetic machine made by a linear array of myosin II motors carried by a structured surface and brought to interact with an actin filament. In this way, the myosin motors work in parallel like in the half-sarcomere and provide the condition for cyclic interactions with the actin filament. The mechanical outputs of this collective motor would be in the range 0.5–200 pN force and 1–10,000 nm movement. To measure and control the mechanical performance of such machines is beyond the possibility of the single-laser optical tweezers considered so far. The range of the needed movement is above what can be attained with AODs, but this limit can overcame keeping fixed the trap position and using a piezo-nanopositioner to move the trapping chamber. The other major limit is the reduced force range of the single laser. This is a general problem that prevents the application of the technique for studying all molecular and intermolecular functions that occur at forces >50 pN, such as unfolding of proteins or structural transitions in nucleic acids, and has given way to the double-laser optical tweezers and to AFM-based mechanics.

AFM has the advantage of high-resolution imaging, but, as far as the applications of interest in this report, has limits in the lower force range sensitivity ($\sim$10 pN) and, because of the large dimension of the probe, in the possibility to discriminate between specific and non-specific interactions.

2 The Dual-Laser Optical Tweezers

The dual-laser optical tweezers technique enhances the upper force limit utilizing two counter-propagating beams [2, 34, 35]. The instrument described here, which operates in a dynamic force range 0.5–200 pN, has been developed in our laboratory to study the structure of DNA and the mechanical performance of a motility system made of an ensemble of myosin motors pulling on an actin filament. In this design, two microscope objectives face each other and focus two separate laser beams to the same spot. Since the scattering force on the bead is approximately the same for each laser, these forces cancel out each other and the axial trap stability is greatly enhanced. The dual-laser optical tweezers can therefore generate higher trapping forces for a given laser power. In this case, the upper force limit reaches 200 pN with 100 mW power, while the beams size can be reduced to fill only partially the back focal plane of the objectives, so that all the photons leaving the trapped bead are efficiently collected with the opposite objective lens and are projected onto a position-sensing photodiode. Under these conditions, the force can be measured by the change in light momentum measured by the deflection of the laser beams (Fig. 2a), a method that has the advantage to depend only on the shift of the refracting object from the equilibrium position and not on the size, shape, and, to a give extent, refractive index of the object [35].

While a single-laser optical tweezers can be constructed using a commercial inverted microscope, a dual-laser instrument is typically custom built from opto-mechanical components. The two laser beams must be aligned to within less than a bead diameter, and the resulting measurements must be corrected for errors due to the drift in the relative beam alignment. Because of these alignment issues, a dual-laser tweezers can hardly be used with beads of diameters less than 1 μm. The bead trapped in the focus of the two laser beams is in a flow-through micro-chamber, the position of which is controlled by means of a low-profile three-axes piezo-stage with capacitive position sensing (Mad City Lab, Madison WI, USA). With this device, the position of the specimen is digitally controlled with the precision of 0.5 nm over a volume range 75 $\times$ 75 $\times$ 50 μm.

Data acquisition and control of the piezoelectric stage are done by means of a NI PCI-6251 board driven by LabVIEW software (National Instruments, Austin TX, USA). Joystick control of the stage allows the instrument to be remotely operated. The electronics of the servo loop is implemented to provide position steps complete in 1 ms.

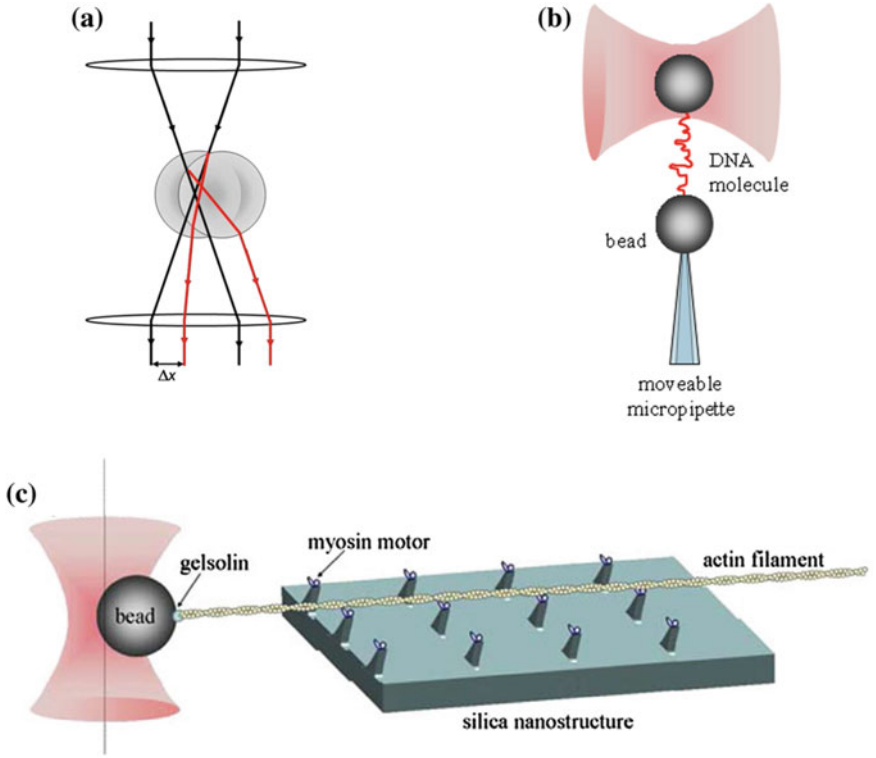

Fig. 2 **a** Change in light momentum (from *black* to *red*) produced by change in the position of the trapped bead and measured by the change in position of the laser beam (Δx) in the back focal plane of the objective. **b** Application of the dual-laser tweezers to mechanics of a DNA molecule (*red*). The ends of the molecule are attached to polystyrene beads one of which is held by suction on the tip of a glass micropipette, while the other is held in the optical trap. **c** Application of the dual-laser tweezers to mechanics of a biomachine made by an array of myosin II motors disposed on a structured silica surface and an actin filament attached with the right polarity (via gelsolin, [36]) to the trapped bead

2.1 Mounting the Specimen in the Experimental Chamber Between the Force and Length Transducers

The flow chamber is assembled by placing two layers of parafilm cut in the chamber shape between two microscope coverslips, to have a chamber depth of 150 μm. The design of the flow chamber is optimized for manipulation and dynamic force and extension measurements of a single double-stranded DNA (ds-DNA) molecule, to determine the kinetics of the overstretching transition from the basic conformation to the 1.7 longer conformation [13, 34]. The chamber is clamped on a holder carried by the piezoelectric stage with two aluminum brackets with threaded holes to connect tubing to the chamber. The flow chamber allows

maintaining a laminar flow that, during the experiment, can be used to provide jumps in the composition of the solution. A micropipette is placed between the two parafilm layers prior to sealing and thus is integral with the flow chamber and the piezo-stage and its position is controlled with sub-nanometer precision. Two streptavidin-coated beads are held: one by the optical trap and the other by the tip of the micropipette through suction (Fig. 2b). A diluted solution of DNA with biotinylated 3' ends is flown through the cell, until one end of a DNA molecule is attached to the trapped bead; then, the bead on the pipette is moved toward the trapped bead until the opposite end of the molecule is bound. Changes in the extension of the molecule are measured by the movements of the two beads. The absolute extension of the molecule is estimated at the end of the experiment by moving the pipette toward the trapped bead and measuring the position of the pipette, with 5-nm precision, when the two beads start to separate as judged from the force signal.

The temperature in the chamber is controlled in the range 4–40 °C by pumping fluid at the desired temperature through copper jackets placed on the objectives [26]. The time to reset the temperature of the solution after solution exchange is 3–5 s. The vibrations due to the fluid circulation pump, tested with power spectrum measurements, are minimized by tightly fitting the jackets around the objectives and by mechanical insulation of the water circulator from the optical table.

For the application of the dual-laser tweezers to the study of the mechanical performance of a motility system made by an ensemble of myosin motors pulling on an actin filament, the design of the chamber and the connections of the specimen to the transducers have to be specifically adapted.

The actin filament is attached with the correct polarity (the barbed or + end) to the bead acting as the force transducer and the structured surface with the array of myosin motors is brought by a support fixed to the chamber carried by the piezo-stage (Fig. 2c).

2.2 Calibration of Force

The force is recorded by the position of the trapped bead, measured by the change in the light momentum (Fig. 2a) with a precision of ~ 0.2 pN. The force calibration is made by determining the trap stiffness in response to known forces of viscous or thermal nature. Actually, to increase the accuracy, the calibration must be done using both viscous drag (1) and thermal noise (2), as follows:

(1) The force due to viscous drag on a sphere of known radius can be calculated according to Stokes' law. If a liquid with viscosity η flows past a sphere of radius R with velocity v, the force due to viscous drag, F_v, is given by:

$$F_v = \gamma v = 6\pi\eta R v, \tag{1}$$

where γ is the viscous drag coefficient. Viscous drag to the trapped bead is applied by moving at preset velocities the flow chamber with the piezo-stage. Because the movement of the flow chamber involves the movement of the entire block of fluid surrounding the trapped bead, the bead is exposed to preset viscous drag forces.

(2) The second technique to calibrate trap stiffness is by measurement of the Brownian motion of the trapped bead. A bead captured in an optical trap experiences random forces due to thermal fluctuations. By Fourier analysis of the positional fluctuations of the trapped bead, the trap stiffness (k) can be directly obtained as

$$k = 2\pi\gamma f_c, \tag{2}$$

where f_c is the corner frequency, the frequency above which the system fails to respond and the position fluctuation is attenuated, as determined by the power spectrum. The viscous drag method involving the movement of the piezo-stage has the advantage of providing a measure of the trap stiffness at large displacements.

2.3 Mechanical Protocols: Length Versus Force Clamp

The instrument can be operated under computer control either as a length clamp, applying length steps or ramps with the three-dimensional piezo-stage connected to one end of the specimen, or as a force clamp, applying abrupt changes in load of fixed magnitude and direction to the trapped bead connected to the other end of the specimen (Fig. 3). In a length clamp experiment, the feedback signal is the position of the piezo-stage and the state of the specimen can be perturbed by lengthening or shortening steps with a risetime ($t_{r,}$ the time to 95 % of the step) that is limited only by the frequency response of the piezo-stage (2.5 kHz in our improved version). In this case, a stepwise perturbation can be much faster than the elicited molecular reaction, allowing the force response to be analyzed in terms of the elastic response, simultaneous with the step, and the following molecular relaxation to the new equilibrium. However, the interpretation of the reaction elicited by the step is complicated by the changes of the potential energy landscape generated by the molecular motion against a changing load. In a force clamp experiment, the feedback signal is the instantaneous position of the trapped bead connected to the other end of the specimen and the feedback system moves the piezo-stage to achieve and maintain a set position of the trapped bead. The force clamp is a very powerful tool and is the protocol of election in the experiments described here, for two important reasons. The first reason is that the molecular or intermolecular process elicited following a step to a given force level occurs in isotonic conditions and thus without the effect of any series compliance between

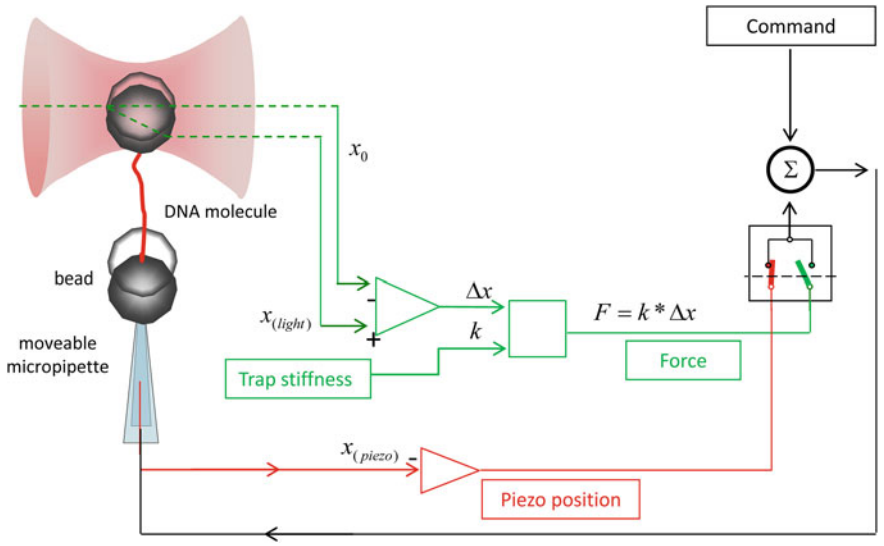

Fig. 3 Block diagram of the electronic circuit that controls the position of the piezo-stage (*black*) in the dual-laser tweezers for DNA mechanics. The summing amplifier (Σ) compares the command with either the force (*green*, calculated by the product of the change in light momentum Δx and the stiffness of the trap k) or the length of the molecule (*red*, measured by the position of the micropipette integral to the piezo-stage, x_{piezo}). The switch selects either the length clamp (position shown) or the force clamp

the specimen and the force transducer (the trap) and the length transducer (the support connected to the piezo-stage), which otherwise would require corrections for the actual movement of the specimen. The second reason is that, following the step, the force and thus the potential energy landscape remain constant and the reaction is followed through the change in length, which serves at the same time as the reaction coordinate. The two-state reaction nature of a given event can be defined by measuring the force dependence of the lifetimes (or rate constants) of the conformational change along the reaction coordinate, and consequently, the relative energy profile and reaction distance can be described.

However, the force clamp suffers of the main limit that the finite response time of the feedback loop (τ_f) reduces the frequency response of the system to <1 kHz. Beyond the frequency response of the piezo-stage, τ_f depends on the trap stiffness, bead size, compliance of tethers connecting the specimen to the transducers, and eventually the specimen compliance. In a recent paper, the problem is described in relation to the folding/unfolding of DNA hairpin (Fig. 4, from Elms et al. [16]). The reduced frequency response in force clamp, with respect to length clamp, causes the failure to record short-lived dwell times in the equilibrium behavior of the two-state reaction. As a consequence, the load dependence of the rate constants obtained from the analysis of the respective lifetimes, interpreted in terms of Bell theory, provides estimates of the distance to the transition state that are

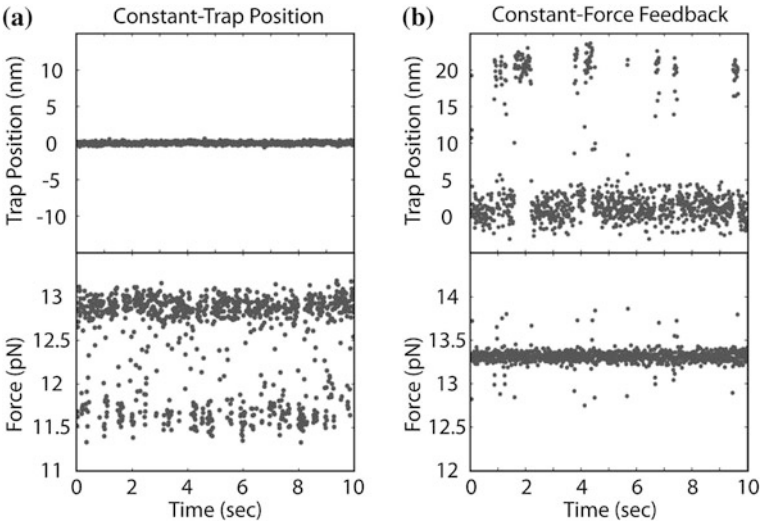

Fig. 4 **a** Record of force fluctuations of a DNA hairpin undergoing folding/unfolding in length clamp. **b** Record of length fluctuations in force clamp. Data averaged down to 100 Hz. From Elms et al. [16]

significantly larger (33 %) than the observed change in the molecular extension. Thus, missing to record the faster events affects the definition of the structure of the reaction producing an overestimate of the reaction distance, and the error increases with the fraction (f_m) of fast events missed. f_m depends on the relative timescales of the molecular reaction under study and the response time of the feedback system τ_f, as defined by:

$$f_m = 1 - \exp\left(-\tau_f k_A \exp\left(\frac{\Delta F_{A-B}\, \Delta x^{\ddagger}}{k_B T}\right)\right) \tag{3}$$

where k_A is the rate constant in state A, ΔF is the change in force between the states A and B, $\Delta x^{\ddagger}$ is the distance to the transition state, k_B is the Boltzmann constant, T is the absolute temperature, and τ_f is the response time of the system. As mentioned above, τ_f depends on the sum of the compliances of the series of elements that constitute the feedback loop, included the compliance of the specimen under study that may change in the different states.

In addition to the limit described above, occurring with force clamp at constant force, there is another major source of error that shows up in force feedback protocols with force steps.

Due to the finite-time limitations of the force feedback, the system can only follow the stepwise command signal on a timescale greater than the timescale of the feedback. Force deviations from the command due to the reaction of the specimen that occurs at shorter timescales would modify the length response in the

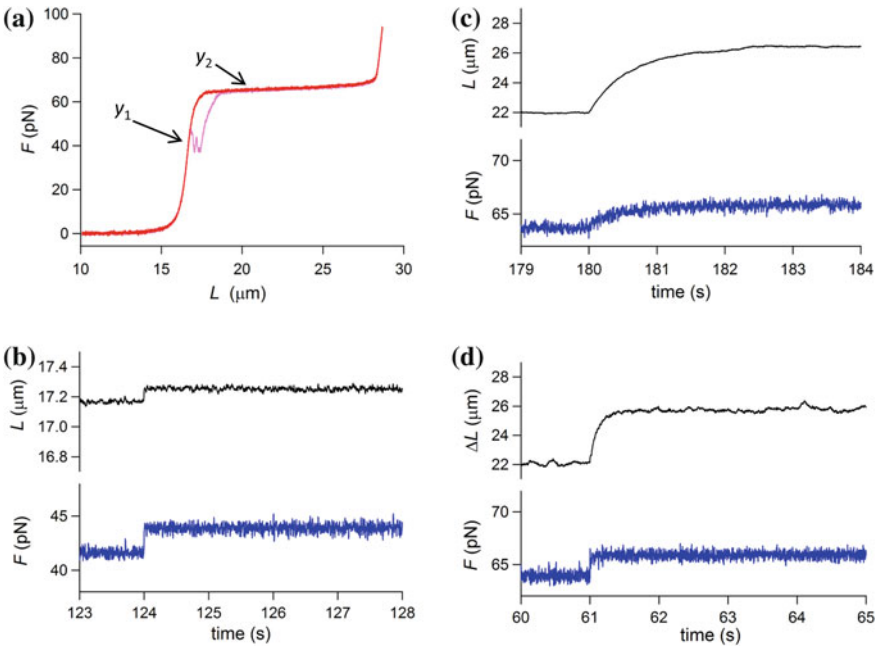

Fig. 5 **a** Force–extension curve of a ds-DNA molecule in physiological solution (150 mM NaCl) and 25 °C. Lengthening (*red*) and shortening (*pink*) are imposed at velocity of 1.4 μm/s. This molecule shows hysteresis under shortening. **b** Length response (*black*) to a 2 pN step (*blue*) imposed on a steady force of 42 pN corresponding to y_1 in **a**. **c** Length response (*black*) to the 2 pN step (*blue*) imposed on a steady force of 63 pN (corresponding to y_2 in a) with the same feedback gain as in **b**. **d** Length response (*black*) to the same step as in **c** (*blue*), but with the feedback gain adjusted to account for the drop in stiffness of the molecule in the overstretching transition region

direction that produces an underestimate of the rate of the length change expected by the commanded force.

To illustrate this point, consider a molecule of ds-DNA on which a force step of 2 pN is superimposed on a steady force level in correspondence of two different regions of the characteristic force–extension (*F–L*) curve (Fig. 5a): y_1(42 pN), in the region of intrinsic elasticity of the molecule, and y_2(63 pN), in the region of the overstretching transition. The command signal has a t_r of 1 ms, and the feedback gain is set for the optimization of the force step ($t_r \sim 2$ ms) in the elastic region. In this case (Fig. 5b), the length response is an almost simultaneous length change of ∼60 nm revealing the elastic properties of the molecule in the basic conformation, with a compliance of ∼30 nm/pN. When the 2 pN step is superimposed on force y_2 (Fig. 5c), the feedback signal is deteriorated, with a t_r that is increased to ∼1 s. The amplitude of the length response is increased by one order of magnitude in comparison with that expected from the compliance in b and has a time course almost parallel to that of the force perturbation. In Fig. 5d, the same

force step command is imposed with the feedback gain, and thus the complex stiffness of the feedback loop, adequately increased to counteract the increased compliance of the molecule in the overstretching region. The consequent reduction in τ_f allows the stepwise shape of the force perturbation to be recovered, which reveals the exponential nature of the lengthening response.

In the experiment described in Fig. 4, fluctuations of a single two-state reaction were recorded, while in the experiment of Fig. 5, we recorded the time evolution of an average over a multitude of copies of the unitary reaction. In this case, the artifact introduced by finite-time limitations of the force feedback consists in an apparent slowing of the transient kinetics (Fig. 5c). Like in the single reaction experiment, in order to check the absence of any artifact in the definition of transient kinetics, the structural information obtained from the transient analysis might be compared with that obtained from a standard equilibrium analysis.

The application of a fast force clamp to the study of the kinetics and energetics of the overstretching transition of ds-DNA is described in the next section, which summarizes the work of Bianco et al. [5].

3 Transition Kinetics of the DNA Elongation Revealed by Force Steps

To describe the coupling between structure and force in ds-DNA is fundamental for understanding the mechanism of the molecular machines used by cells to duplicate and repair their genome and modulate the accessibility of the genetic information [1, 9]. When stretched under forces lower than 60 pN, ds-DNA maintains its basic conformation (B-form) and displays the elastic response of an extensible worm-like chain [8, 27, 33, 43]. At forces higher than 60 pN, the molecule abruptly becomes much more extensible (overstretching transition) and within a few piconewtons acquires an extended conformation (S-form) 1.7 times longer than the B-form [13, 34].

Although the overstretching phenomenon has long been known, a detailed description of its mechanism is still missing. There are contributions [29, 30, 32, 40, 44, 46, 47] in favor of the idea that the elongation could merely be due to a force-induced melting with strand separation, as indicated by the hysteretic behavior in consecutive stretching and shortening cycles. However, other experiments support the view that overstretched DNA is characterized by a reduced helicity [7, 22, 31] with a stiffness higher than expected for single stranded (ss-) DNA [14, 45]. In this case, melting should occur at nicks in the phosphate backbone [34, 43] or at the free DNA ends, by an extent that depends on the bp sequence, solution conditions and manipulation of the molecule [12, 15, 19, 20, 40, 47]. In particular, it has been shown in force clamp experiments [19, 20] that DNA overstretching under melting-preventing conditions (such as high salt concentration, GC-rich sequences) involves only a rapid non-hysteretic transition to the

elongated double-stranded S-form, while removing these conditions induces also a slow hysteretic strand separation.

All the above studies have a limit in defining the nature of the overstretching transition, because they use the equilibrium force–extension relation and do not have the time resolution for determining the non-equilibrium kinetics. The development of our dual-laser tweezers with a sufficiently fast force clamp has provided for the first time the opportunity for recording the length transient elicited by force steps and its dependence on the load, providing the constraints for the definition of the structure of the unitary reaction.

In the experiment of Fig. 6a, a staircase of force steps of amplitude 2 pN is imposed on a molecule of ds-DNA with ends opened and kept in a solution with physiological salt composition and room temperature. In the region of the overstretching transition (between 60 and 72 pN, Fig. 6b), the length response to a 2 pN step is characterized by an exponential time course (Fig. 6c), which implies per se that the main transition mechanism cannot be force-induced melting starting at the free ends and then propagating inward [40], since this process would be characterized by linear kinetics.

Five to eight steps of 2 pN are necessary to complete the B–S transition. Superposing the elongations elicited by a series of six 2-pN steps, identified in Fig. 6c by the different colors, it can be seen how the amplitude and the speed of the response depend on the force attained at the end of each step. Going from the first (purple) to the sixth (green) step, the amplitude of the elongation (ΔL_e) increases abruptly up to a maximum of $\sim$3.3 μm (third step, black) and then reduces again. After the elastic response has been subtracted, the time course of the elongation (ΔL) is fitted with the exponential equation $\Delta L = \Delta L_e \cdot (1 - \exp(-rt))$, where t is the time elapsed after the step, r is the rate constant, and ΔL_e is the asymptotic value of the elongation. ΔL_e is smaller, and r is larger at the beginning and at the end of the B–S transition. The dependence of r on the force attained after the 2 pN step, shown by blue symbols in Fig. 6d, is U-shaped, showing maxima of $\sim$50 s^{-1} at the beginning ($F \sim 62$ pN) and at the end ($F \sim 72$ pN) of the overstretching transition and a minimum of 3.82 ± 0.68 s^{-1} (mean and SD, calculated in the range 65.5–66.5 pN) in the plateau region. If the size of the step is reduced to 0.5 pN, the amplitude of the elongation response reduces and the number of steps necessary to complete the B–S transition increases, but the r–F points (green circles) superpose on those obtained with 2 pN steps (blue symbols). Thus, the r–F relation depends uniquely on the final force attained by the step and is independent of the size of the step and, moreover, of the occurrence of some degree of melting, as shown by the hysteresis upon relaxation (compare blue squares, from 4 molecules without hysteresis, and triangles, from the 13 molecules with hysteresis).

In force clamp experiments with the dual-laser tweezers apparatus, the length change elicited by a force step is realized through movement of the piezo-stage and thus of the fluid surrounding the bead. Consequently, the change in position of the trapped bead reliably measures the tension on the molecule only if it is not influenced by a significant drag due to the movement of the solution accompanying

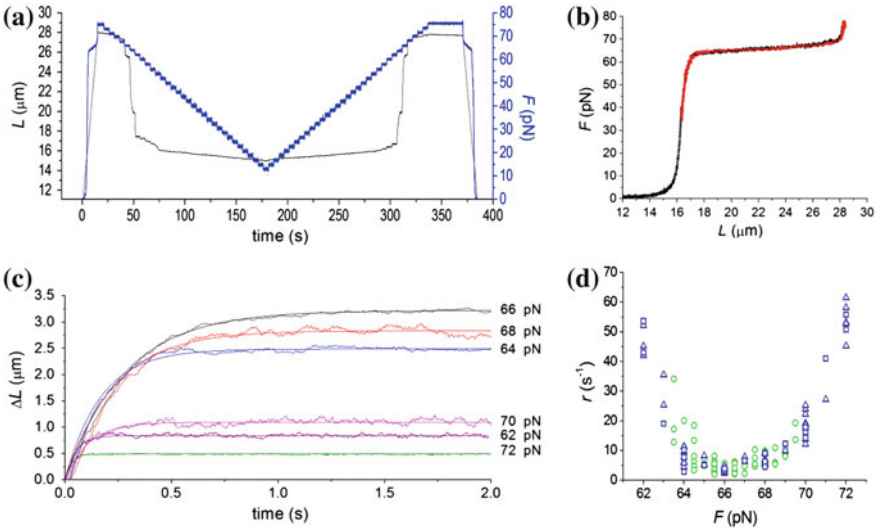

Fig. 6 **a** Time course of the length (*black*) and force (*blue*) of ds-DNA first stretched in length clamp (velocity 1.4 μm/s) then shortened in force clamp with a staircase of 2 pN steps at 5 s interval, then stretched again with a similar staircase of 2 pN steps and eventually shortened in length clamp at velocity 1.4 μm/s. **b** Force–extension curves in length clamp (*black*) and in force clamp (*red*) drawn from a protocol like that in **a** for a molecule without hysteresis. **c** Superimposed time courses of elongation (ΔL) following a series of 2 pN force steps starting at 60 pN during the staircase. The level of force attained by the step is reported next to the trace. The lines are single exponential fits to the traces. **d** Relationship between the rate of elongation (r) and force attained at the end of the step (F) following 0.5 pN (*green circles*) and 2 pN (*blue symbols*) steps. 2 pN data are from 13 molecules showing hysteresis in relaxation (*triangles*) and 4 molecules without hysteresis (*squares*). From Bianco et al. [5]

the movement of the stage. Moreover, there may be a significant rotational drag while ds-DNA elongates/untwists during the overstretching transition, which could affect the rate of elongation. All these problems are discussed in detail in the Appendix, showing the absence of any significant influence of viscosity. Under these conditions, the *r–F* relation is an intrinsic property of the molecule, related to its transition kinetics.

4 The Structure of the DNA Overstretching Transition

The results of non-equilibrium kinetics just described are the basis for the definition of a two-state reaction model that predicts the structure of the overstretching transition. The model assumes that ds-DNA is composed of an ensemble of units which can attain two different conformational states, a compact B state (with a

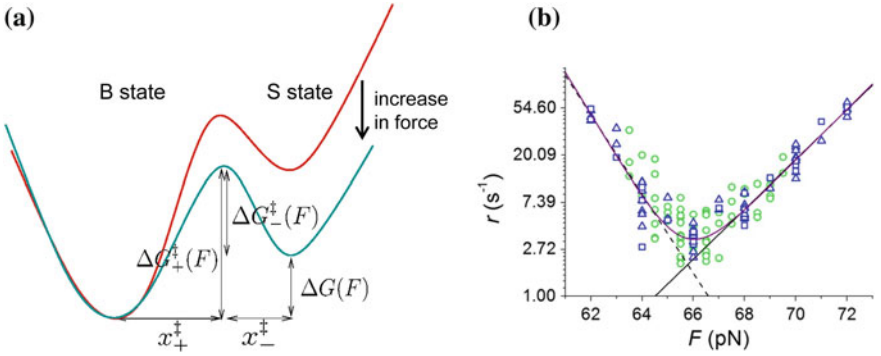

Fig. 7 **a** Free-energy profile of a two-state unit and the effect of an external force (from *red* to *blue*). The force *tilts* the energy landscape and thus lowers the energy barrier for the transition to the extended state. $\Delta G_+^{\ddagger}$, energy barrier for the forward transition; $\Delta G_-^{\ddagger}$, energy barrier for the backward transition; ΔG, free-energy difference between the two states. The transition state distance is $x_+^{\ddagger}$ from the B state and $x_-^{\ddagger}$ from the S state. **b** Relation between ln r and F. (*Black straight lines*): Fits of Eq. 7 (*continuous line*) to data in the force range 67–72 pN and Eq. 8 (*dashed line*) to data in the range 61–65 pN. (*Purple line*) four-parameter fit with Eq. 9 to all data. From Bianco et al. [5]

molecular extension of 0.33 nm per bp) and an extended S state (with a molecular extension of 0.56 nm per bp). The molecular extension of each of these units provides a convenient reaction coordinate to study the overstretching transition. The free-energy profile of each unit along this reaction coordinate, schematically represented in Fig. 7a, is dictated by four fundamental parameters: the free-energy difference between B and S states ΔG, the forward energy barrier $\Delta G_+^{\ddagger}$ (the backward barrier $\Delta G_-^{\ddagger}$ being $= \Delta G_+^{\ddagger} - \Delta G$), and the distances of the transition state from both the B state $x_+^{\ddagger}$ and the S state $x_-^{\ddagger}$.

When a force F is applied to the molecule, the free-energy profile tilts (from red to blue in Fig. 7a), leading to a decrease in the free-energy difference ΔG and a decrease of the free-energy barrier for stretching and a corresponding increase of the free-energy barrier for shortening:

$$\Delta G_{\pm}^{\ddagger} = \Delta G_{\pm}^{\ddagger} \mp F x_{\pm}^{\ddagger}. \tag{4}$$

The rate constants for the elongation (k_+) and the shortening (k_-) of the molecule depend exponentially on the force according to Kramers–Bell theory [4, 17, 21]:

$$k_+ = A_+ \cdot \exp\left(\frac{F \cdot x_+^{\ddagger}}{k_B T}\right) \tag{5}$$

$$k_- = A_- \cdot \exp\left(-\frac{F \cdot x_-^{\ddagger}}{k_B T}\right), \tag{6}$$

where k_B is the Boltzmann constant, T is the temperature in Kelvin, and A_+ and $A_-(s^{-1})$ are the rate constants at zero force.

The unidirectional rate constants expressed in logarithmic units have a linear dependence on force, and the slope of the relation is the distance from the starting state to the transition state divided by $k_B T$:

$$\ln k_+ = \ln A_+ + \left(\frac{F \cdot x_+^{\ddagger}}{k_B T}\right) \tag{7}$$

$$\ln k_- = \ln A_- - \left(\frac{F \cdot x_-^{\ddagger}}{k_B T}\right). \tag{8}$$

In our experiments, the observed rate constant r (Fig. 6d) is the sum of the forward and backward rate constants. However, since the equilibrium is dominated by k_- in the low force side of the overstretching transition and by k_+ in the high force side, we used the logarithmic relations in these two regions to separately estimate the slopes of the respective unidirectional reactions and thus of the distances to the transition state (Fig. 7b). The parameters of the linear regression equations fitted to ln r with Eq. 7 in the force range 67–72 pN and Eq. 8 in the range 61–65 pN are reported in Table 1 either for the 0.5 pN steps (green circles) or for the 2 pN steps (blue symbols). It can be seen that all the kinetic parameters are not significantly influenced by the force step size ($P > 0.1$). The linear fits on the pooled 0.5 and 2 pN data within the same force ranges give similar values.

Alternatively, a more complex, four-parameter fit with the expression

$$r = k_+ + k_- = A_+ \exp\left(\frac{F x_+^{\ddagger}}{k_B T}\right) + A_- \exp\left(\frac{F x_-^{\ddagger}}{k_B T}\right) \tag{9}$$

can be performed on the entire force range (purple line in Fig. 7b) and gives values of the four parameters A_+, A_-, $x_+^{\ddagger}$, and $x_-^{\ddagger}$ (Table 1) that are almost identical to those determined by fitting separately the low and high force branch of the relation.

The distances to the transition state, $x_+^{\ddagger}$ and $x_-^{\ddagger}$, are similar showing that the transition occurs roughly midway between the B state and the S state of DNA, slightly shifted toward the B state. The sum of the two distances, $\left(x_-^{\ddagger} + x_-^{\ddagger}\right)$, gives a total length change of 5.85 ± 0.20 nm for the unitary reaction Δx. The ratio of Δx over the elongation undergone by each bp ($0.33 \times 1.7 - 0.33 = 0.231$ nm)

Table 1 Kinetic parameters of the two-state reaction estimated with Eqs. 7 and 8 (first three rows) and with Eq. 9 (fourth row)

	$\ln A_+$	$x_+^{\ddagger}$ (nm)	$\ln A_-$	$x_-^{\ddagger}$ (nm)
0.5 pN step	-32 ± 7	2.1 ± 0.4	64 ± 12	3.9 ± 0.8
2 pN step	-34.4 ± 1.3	2.18 ± 0.07	61 ± 3	3.7 ± 0.2
Pooled	-34.1 ± 1.1	2.18 ± 0.07	56 ± 3	3.7 ± 0.2
Pooled, four parameters	-34.1 ± 1.7	2.2 ± 0.1	59 ± 4	3.7 ± 0.2

measures the number of bp involved in the unitary reaction, or cooperativity coefficient, and is 25.32 ± 0.86.

The finding that the transition state is almost midway between the compact and extended states implies that the force (F_m) at which the relaxation rate is minimum also corresponds, within our resolution limit, to the force (F_e) at which the work done for the elongation (W_e) equals the free-energy difference between the compact and the extended states: $W_e = F_e \times \Delta x$. With $\Delta x = 5.85$ nm, W_e is ($66 \times 5.85 =$) 386 zJ per molecule (or 236 kJ per mol), that at 25 °C corresponds to 94 k_BT. The average binding free energy per bp obtained from these mechanical measurements is ($F_e \times 0.231$ nm =) 15.25 zJ, corresponding to only 3.71 k_BT per molecule. Thus, the cooperative mechanism for DNA elongation increases the stability of the DNA structure in the B state by increasing the minimal free-energy change necessary for the elongation reaction to 94 k_BT.

5 Assessing the Force Clamp Description of DNA Overstretching Kinetics: Comparison Between Non-equilibrium and Equilibrium Results

As demonstrated by Elms et al. [16] for a single two-state reaction (Fig. 4), also for the time course of a multitude of copies of the unitary reaction finite-time limitations of the force feedback would produce an apparent slowing of the length transient. To check the absence of any artifact in the definition of transient kinetics, here the structural information obtained from non-equilibrium analysis is compared with that obtained from equilibrium analysis.

The unidirectional transition rates between the two conformations k_+ and k_- depend on an additional parameter Ω, a kinetic pre-factor which is related to the viscous drag experienced by the molecule in its motion along the reaction coordinate and to the shape of the molecular potential energy near the transition state. According to Kramers-Bells theory, the A_+ and A_- parameters are:

$$A_+ = \Omega \exp\left(-\frac{\Delta G_+^{\ddagger}}{k_B T}\right) \tag{10}$$

and

$$A_{-} = \Omega \exp\left(-\frac{\Delta G_{+}^{\ddagger} - \Delta G}{k_{\mathrm{B}}T}\right) \tag{11}$$

The force (F_{m}) corresponding to the minimal relaxation rate $r(F)$ is

$$F_{\mathrm{m}} = \frac{\Delta G - k_{\mathrm{B}}T \ln\left(x_{+}^{\ddagger}/x_{-}^{\ddagger}\right)}{x_{+}^{\ddagger} + x_{-}^{\ddagger}} = F_{\mathrm{e}} - \frac{k_{\mathrm{B}}T \ln\left(x_{+}^{\ddagger}/x_{-}^{\ddagger}\right)}{x_{+}^{\ddagger} + x_{-}^{\ddagger}} \tag{12}$$

where F_{e} is the coexistence force, the force at which the probabilities to reside in the B and S state (p_{B} and p_{S}) are equal.

Also, the equilibrium probabilities at each force are known:

$$p_{\mathrm{B}}(F) = \frac{1}{1 + \exp\left(-\frac{\Delta G - F\left(x_{+}^{\ddagger} + x_{-}^{\ddagger}\right)}{k_{\mathrm{B}}T}\right)} \tag{13}$$

and

$$p_{\mathrm{S}}(F) = \frac{\exp\left(-\frac{\Delta G - F\left(x_{+}^{\ddagger} + x_{-}^{\ddagger}\right)}{k_{\mathrm{B}}T}\right)}{1 + \exp\left(-\frac{\Delta G - F\left(x_{+}^{\ddagger} + x_{-}^{\ddagger}\right)}{k_{\mathrm{B}}T}\right)} \tag{14}$$

$p_{\mathrm{S}}(F)$ grows monotonically with F, having maximal first derivative at the coexistence force, $F_e = \Delta G/\left(x_{+}^{\ddagger} + x_{-}^{\ddagger}\right)$. At this force $\Delta G = F \cdot \left(x_{+}^{\ddagger} + x_{-}^{\ddagger}\right)$, that is, the work done for the elongation equals the free-energy difference between the B and the S state. We note that only for symmetric landscapes, $x_{+}^{\ddagger} = x_{-}^{\ddagger}$, F_{e} coincides with F_{m}, the force of minimal relaxation rate.

During a positive staircase of force steps, when the force is changed from F to $F + \Delta F$, the probability to be in the extended state grows and, after equilibration, $N(p_S(F + \Delta F) - p_S(F))$units have extended, where N is the total number of extensible units. It is therefore straightforward to compute the equilibrium force–extension profile which, according to the expressions for p_S and p_B, depends only on the two parameters ΔG and $x_+ + x_-$. In Fig. 8, the experimental force–extension relation (black trace) from Fig. 6b is compared to the theoretical relation (red dashed line) obtained with the ΔG and $x_+ + x_-$ chosen by fitting the elongation rates with the procedure described in the test. The agreement shows that the model developed to fit the observed relaxation kinetics is capable of reproducing the equilibrium force–extension relation, proving that our force clamp has the time resolution for correctly recording the transient elicited by force steps.

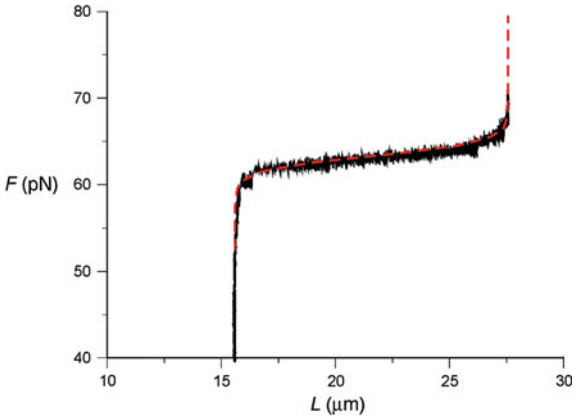

Fig. 8 Comparison between the experimental equilibrium force–extension relation (*black traces*) and the simulated relation (*red dashed trace*), calculated with the parameters extracted from the transient kinetics analysis of the responses to force steps. The base pair separations in states B and S were set to 0.325 and 0.57 nm, respectively. From Supplementary material in Bianco et al. [5]

Eventually, it is worth assessing whether the exponential kinetics observed for λ-DNA contrasts with the results of other recent overstretching experiments under force clamp. Fu et al. [19] report on constant force DNA overstretching experiments performed by means of magnetic tweezers. Under melting-preventing conditions (high salt concentration or moderately GC-rich sequences), DNA constructs of approximately 600 bp show, in response to force increase, discrete lengthening steps followed by length fluctuations, instead of a smooth exponential elongation (Fig. 9a). The predictions of our two-state model for such conditions are tested by performing a series of Monte Carlo simulations. A set of 23 two-state units, each 25 bp long, was defined in order to simulate a molecule 575 bp long. All units were initially assigned a compact conformation, and force was gradually increased with 1 pN steps. For each force value, the system was integrated for 20 s according to a stochastic dynamics where each unit could change its state from compact to extended and from extended to compact according to their transition probabilities computed as $k_{\pm}\,\mathrm{d}t$ with dt the integration time. $k_{\pm}$ were computed according to Eqs. 5 and 6, using the parameters resulting from the fit of the rate–force relation as in Fig. 6d. Figure 9b confirms that, for a molecular size as low as 575 bp, random length fluctuations are so prevalent to mask almost completely the shape of the relaxation. On the contrary, as shown in Fig. 9c, that reports the result of a simulation with 1,936 two-state units, or (1,936 × 25 =) 48,400 bp, the entire DNA molecule exhibits a much smoother lengthening, that with an adequately expanded timescale (Fig. 9d), reveals its exponential kinetics. This is due to the

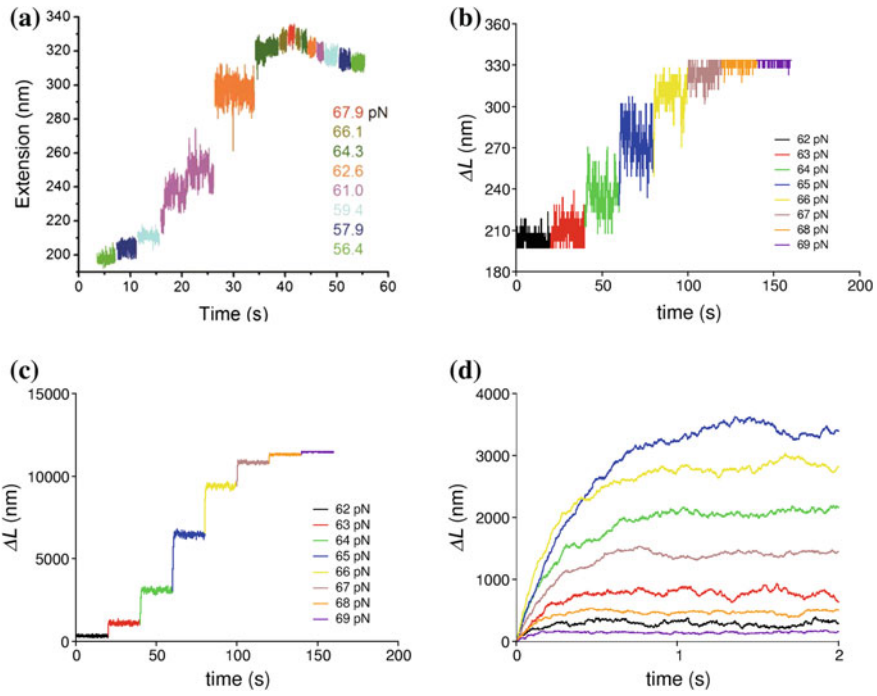

Fig. 9 **a** Length response to a staircase of force increments of ∼1.5 pN imposed on a DNA construct of ∼600 bp under melting-preventing conditions throughout the overstretching transition region (corresponding force attained by the step identified by the colors, pH 7.5, 24 °C). From Fu et al. [20]. **b** Simulated length responses to eight consecutive force steps of 1 pN (force attained by the step identified by the colors) imposed on 23 identical two-state units of 25 bp (total number of bp 575). **c** Simulated length responses to eight consecutive force steps of 1 pN as in **b**, imposed on 1,936 two-state units of 25 bp (total number of bp 48,400). **d** Superposed length responses as in **c**, on a faster time base, adequate to resolve the exponential time course of the early phase of the response, similar to the experimental responses in Fig. 6c. This indicates that the stepwise length changes in **a** are due to the absence of time resolution in those experiments. **b–d** From Bianco et al. [5]

self-averaging effect of length fluctuations in the units in a linear chain when the number of units is sufficiently high: for each extending unit another one contracts compensating the effect of the first. A striking result of this simulation is that the number of bp involved in the elementary reaction (25, the cooperativity coefficient), selected for fitting the responses of a molecule 48 kbp long with the two-state model, is able to predict to a very good approximation the length fluctuations measured by Fu and coworkers for molecules two orders of magnitude shorter.

Appendix: Influence of Viscosity on the Kinetics of the Elongation–Untwisting of the ds-DNA During the Overstretching Transition

Drag Produced on the Trapped Bead by the Viscosity of the Medium

A general problem with force clamp experiments made using the dual-laser tweezers apparatus is that the length change elicited by a force step is realized through movement of the piezo-stage and thus of the fluid surrounding the bead. Consequently, the change in the position of the trapped bead reliably measures the tension on the molecule only if it is not influenced by the drag due to the movement of the solution accompanying the movement of the stage. The drag on the bead is $F_v = 6\,\pi\,\eta\,R v$ (Eq. 1), where η, the viscosity of the solution, is 10^{-3} Pa s, at 25 °C, R, the radius of the bead, is 1.64 or 1.09 μm, and v is the translational velocity of the bead. Considering that the stiffness of the molecule is $\sim$60 pN μm^{-1} and the stiffness of the trap is 150 pN μm^{-1}, a step of 2 pN complete in 2 ms implies a bead movement of $\sim$40 nm at a velocity of $\sim$20 μm s^{-1}. Consequently, for the bead with $R = 1.09$ μm, F_v attains a value of 0.5 pN and decays with a time constant of 0.5 ms (1/4 the risetime of the step). This analysis indicates that the viscous drag on the bead does not significantly influence the position of the bead during the step nor the observed elongation kinetics.

A direct test of this conclusion is obtained by comparing the r–F relations obtained with different bead diameters. In Fig. 10a, the blue points data from Fig. 7c are unpooled to identify those obtained with beads of 3.28 μm diameter (black symbols, 12 molecules) and 2.18 μm diameter (red symbols, 5 molecules). Moreover, in Fig. 10b, r is plotted on a log–log scale against the final length change (ΔL_e) induced by a step, for the same data as in a. In both cases, it is evident the absence of any effect of the bead diameter on the overstretching kinetics.

Rotational Drag of the Molecule While Untwisting

A rotational drag of the ds-DNA while untwisting in response to a rise in torque has been directly measured by attaching a bead near a nick and determining the angular velocity [7]. In this way, it has been shown that the untwisting takes several minutes and the drag dominates the elongation–untwisting velocity. However, in that experiment, the drag should be several times larger than in our experiment, as it is generated by the revolutions of a large bead accompanying the untwisting of the molecule.

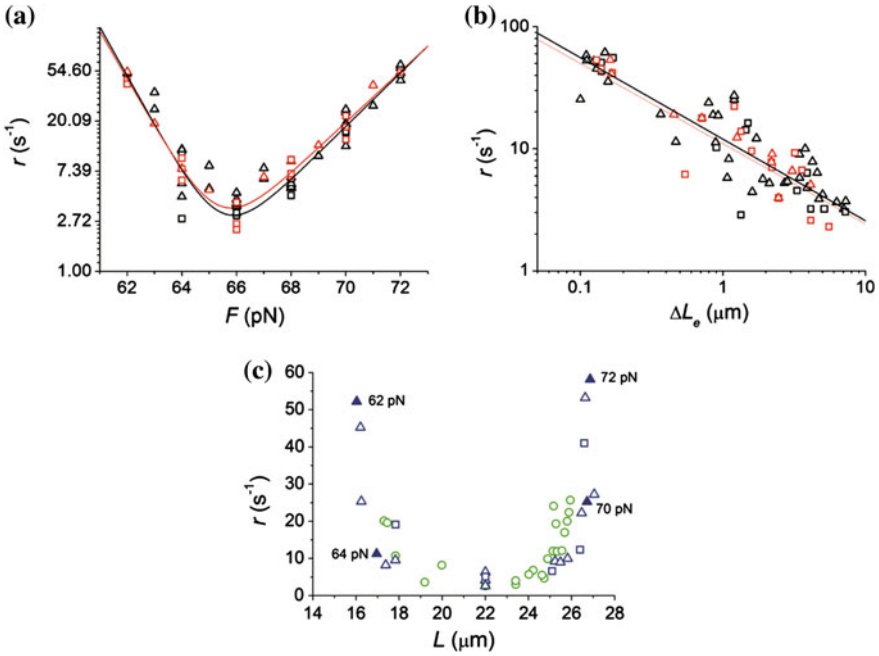

Fig. 10 **a** Relation of ln *r* versus *F* for the 2 pN steps (*blue symbols*) from Fig. 7b. *Red symbols* refer to data obtained with 2.18 μm bead diameter (5 molecules); *black symbols* to data obtained with 3.28 μm bead diameter (12 molecules). **b** Log–log relation between *r* and amount of lengthening (ΔL_e) for the same 2 pN steps as in **a**. **c** Relation of *r* versus the total molecular length (*L*) attained following 0.5 pN (*green circles*) and 2 pN (*blue symbols*) steps. 2 pN data pooled from the same molecules as in Fig. 6d. Figures close to *filled symbols* indicate the respective forces. From Supplementary Material in Bianco et al. [5]

During the overstretching transition under our conditions, the molecule of DNA elongates by 11 μm, while it reduces the number of turns from 4,500 to 1,450, that is, it untwists by 278 turns μm^{-1}. The largest elongation in response to a 2 pN step is ∼5 μm attained within 0.5 s (Fig. 6). This implies a rotational speed ω of (278 × 5/0.5 =) 2,780 turns s^{-1}, so that each of the two ends of the molecule should counter-rotate at 1,390 turns s^{-1}. According to measurements of rotational drag in the experiment of Thomen et al. [39], where the two strands of DNA are attached to two independent beads and separated at different velocities, a torque of 0.6 $k_B T$ would be necessary for the rotation at the speed of our overstretching transition. However, in that experiment, the rotating stretch is at longitudinal force zero (and therefore, the molecule is not straight), while during the overstretching transition, the longitudinal force is ∼65 pN and the molecule can be assimilated to a rigid rod. Modeling a rigid rod [23] leads to a torque $\vartheta = 4\pi\eta R_H^2 L_{\text{eff}}\,\omega$, where η is the viscosity of the solution as above, R_H the hydrodynamic radius of DNA (1.05 nm, [39]), and L_{eff} the extension of the portion of DNA which rotates in order to release the torsional stress. The molecular extension in the middle of the

plateau of the overstretching transition is approximately 22 μm which, under the assumption of torsional stress accumulating in the middle of the molecule, gives a L_{eff} of 11 μm. With $\omega = 1{,}390$ turns s^{-1} (= 8,730 rad s^{-1}), the maximal frictional torque results to be 0.3 k_BT. If, however, the torsional stress is distributed uniformly along the whole length of the molecule, the resulting frictional torque should drop to 0.15 k_BT. A frictional reaction of 0.15–0.3 k_BT is expected to have a negligible effect on the kinetics of the B–S transition as demonstrated below.

The presence of an external torque (in this case of frictional origin) opposing the B–S transition not only modifies the free-energy difference between S and B states but also the free-energy barriers that the system must overcome for the transition (Fig. 7a). The B–S barrier will be increased (more difficult transition), while the S–B barrier will be decreased (easier transition). Let us define x_B and x_S the distances between consecutive bps in the two states and θ_B and θ_S the twist angles between consecutive bps, with numerical values: $x_B = 0.34$ nm, $x_S = 0.58$ nm $\theta_B = 1/10$ turns $= 0.63$ rad, $\theta_S = 1/30$ turns $= 0.21$ rad. Assuming for simplicity that the transition state is in the middle between both x_S and x_B and θ_S and θ_B, the change in barrier height due to the presence of a viscous torque can be estimated and compared with the analogous change due to the presence of an external force. The maximum torque-induced barrier change is $\Delta E_\tau = \tau(\theta_S - \theta_B)/2 = 0.3\ k_BT \times 0.4/2 = 0.25$ pN nm or 0.06 k_BT, while the barrier change caused by the external force F ($\sim$65 pN at the transition) is $\Delta E_F = F(x_S - x_B)/2 = 65 \times 0.24/2 = 7.8$ pN nm or 1.9 k_BT. Thus, since the barrier change introduced by the viscous torque is smaller by a factor of 32 relative to the barrier change caused by the external force, the torsional viscosity contribution can be disregarded.

A simple direct test of the influence of the rotational drag of the molecule on the kinetics of elongation is obtained by plotting the elongation rate r as a function of the length of the molecule L during the overstretching transition (Fig. 10c). If the elongation kinetics was dominated by the viscous friction, one would expect the relaxation rates to depend on L. Actually, the r–L relation shows a U-shaped dependence that excludes the hypothesis of a significant effect of the rotational drag on the elongation rate.

A further test is provided by the comparison of the responses to 2 and 0.5 pN force steps. For the same force, the extent of elongation (and thus ω) is smaller with the smaller step . Since the rotational drag depends linearly on ω, if it was dominating the kinetics of the process, it would have generated a reduction of the rate constant of elongation for the larger step. However, the observed rate constant is the same at the same force for either step size (Fig. 6d, blue 2 pN, green 0.5 pN).

In conclusion, both the theoretical treatment and the experimental evidences given above support the conclusion that the rate of DNA elongation following force steps applied in the overstretching transition region is not affected by viscosity and is mainly determined by the kinetics of the two-state reaction.

References

1. Allemand JF, Bensimon D, Croquette V (2003) Stretching DNA and RNA to probe their interactions with proteins. Curr Opin Struct Biol 13:266
2. Ashkin A (1970) Acceleration and trapping of particles by radiation pressure. Phys Rev Lett 24:156
3. Ashkin A, Dziedzic JM, Bjorkholm JE, Chu S (1986) Observation of a single-beam gradient force optical trap for dielectric particles. Opt Lett 11:288
4. Bell GI (1978) Models for the specific adhesion of cells to cells. Science 200:618
5. Bianco P, Bongini L, Melli L, Dolfi M, Lombardi V (2011) Piconewton-millisecond force steps reveal the transition kinetics and mechanism of the double-stranded DNA elongation. Biophys J 101:866
6. Block SM, Goldstein LS, Schnapp BJ (1990) Bead movement by single kinesin molecules studied with optical tweezers. Nature 348:348
7. Bryant Z, Stone MD, Gore J, Smith SB, Cozzarelli NR, Bustamante C (2003) Structural transitions and elasticity from torque measurements on DNA. Nature 424:338
8. Bustamante C, Marko JF, Siggia ED, Smith S (1994) Entropic elasticity of lambda-phage DNA. Science 265:1599
9. Bustamante C, Bryant Z, Smith SB (2003) Ten years of tension: single-molecule DNA mechanics. Nature 421:423
10. Capitanio M, Canepari M, Cacciafesta P, Lombardi V, Cicchi R, Maffei M, Pavone FS, Bottinelli R (2006) Two independent mechanical events in the interaction cycle of skeletal muscle myosin with actin. Proc Natl Acad Sci USA, vol 103
11. Capitanio M, Canepari M, Maffei M, Beneventi D, Monico C, Vanzi F, Bottinelli R, Pavone FS (2012) Ultrafast force-clamp spectroscopy of single molecules reveals load dependence of myosin working stroke. Nat Methods 9:1013
12. Clausen-Schaumann H, Rief M, Tolksdorf C, Gaub HE (2000) Mechanical stability of single DNA molecules. Biophys J 78:1997
13. Cluzel P, Lebrun A, Heller C, Lavery R, Viovy JL, Chatenay D, Caron F (1996) DNA: an extensible molecule. Science 271:792
14. Cocco S, Yan J, Leger JF, Chatenay D, Marko JF (2004) Overstretching and force-driven strand separation of double-helix DNA. Phys Rev E Stat Nonlin Soft Matter Phys 70:011910-1
15. Danilowicz C, Limouse C, Hatch K, Conover A, Coljee VW, Kleckner N, Prentiss M (2009) The structure of DNA overstretched from the 5'5' ends differs from the structure of DNA overstretched from the 3'3' ends. Proc Natl Acad Sci USA 106:13196
16. Elms PJ, Chodera JD, Bustamante CJ, Marqusee S (2012) Limitations of constant-force-feedback experiments. Biophys J 103:1490
17. Evans E (2001) Probing the relation between force - lifetime - and chemistry in single molecular bonds. Annu Rev Biophys Biomol Struct 30:105
18. Finer JT, Simmons RM, Spudich JA (1994) Single myosin molecule mechanics: piconewton forces and nanometre steps. Nature 368:113
19. Fu H, Chen H, Marko JF, Yan J (2010) Two distinct overstretched DNA states. Nucleic Acids Res 38:5594
20. Fu H, Chen H, Zhang X, Qu Y, Marko JF, Yan J (2011) Transition dynamics and selection of the distinct S-DNA and strand unpeeling modes of double helix overstretching. Nucleic Acids Res 39:3473
21. Kramers HA (1940) Brownian motion in a field of force and the diffusion model of chemical reactions. Physica 7:284
22. Léger JF, Romano G, Sarkar A, Robert J, Bourdieu L, Chatenay D, Marko JF (1999) Structural Transitions of a Twisted and Stretched DNA Molecule. Phys Rev Lett 83:1066
23. Levinthal C, Crane HR (1956) On the Unwinding of DNA. Proc Natl Acad Sci USA 42:436
24. Liphardt J, Onoa B, Smith SB, Tinoco I Jr, Bustamante C (2001) Reversible unfolding of single RNA molecules by mechanical force. Science 292:733

25. Mallik R, Carter BC, Lex SA, King SJ, Gross SP (2004) Cytoplasmic dynein functions as a gear in response to load. Nature 427:649
26. Mao H, Arias-Gonzalez JR, Smith SB, Tinoco I Jr, Bustamante C (2005) Temperature control methods in a laser tweezers system. Biophys J 89:1308
27. Marko JF, Siggia ED (1995) Stretching DNA. Macromolecules 28:8759
28. Perkins TT, Dalal RV, Mitsis PG, Block SM (2003) Sequence-dependent pausing of single lambda exonuclease molecules. Science 301:1914
29. Rouzina I, Bloomfield VA (1999) Heat capacity effects on the melting of DNA. 1. General aspects. Biophys J 77:3242
30. Rouzina I, Bloomfield VA (1999) Heat capacity effects on the melting of DNA. 2. Analysis of nearest-neighbor base pair effects. Biophys J 77:3252
31. Sarkar A, Leger JF, Chatenay D, Marko JF (2001) Structural transitions in DNA driven by external force and torque. Phys Rev E Stat Nonlin Soft Matter Phys 63:051903-1
32. Shokri L, Marintcheva B, Eldib M, Hanke A, Rouzina I, Williams MC (2008) Kinetics and thermodynamics of salt-dependent T7 gene 2.5 protein binding to single- and double-stranded DNA. Nucleic Acids Res 36:5668
33. Smith SB, Finzi L, Bustamante C (1992) Direct mechanical measurements of the elasticity of single DNA molecules by using magnetic beads. Science 258:1122
34. Smith SB, Cui Y, Bustamante C (1996) Overstretching B-DNA: the elastic response of individual double-stranded and single-stranded DNA molecules. Science 271:795
35. Smith SB, Cui Y, Bustamante C (2003) Optical-trap force transducer that operates by direct measurement of light momentum. Methods Enzymol 361:134
36. Suzuki N, Miyata H, Ishiwata S, Kinosita K Jr (1996) Preparation of bead-tailed actin filaments: estimation of the torque produced by the sliding force in an in vitro motility assay. Biophys J, vol 70
37. Svoboda K, Schmidt CF, Schnapp BJ, Block SM (1993) Direct observation of kinesin stepping by optical trapping interferometry. Nature 365:721
38. Svoboda K, Block SM (1994) Force and velocity measured for single kinesin molecules. Cell 77:773
39. Thomen P, Bockelmann U, Heslot F (2002) Rotational drag on DNA: a single molecule experiment. Phys Rev Lett 88:248102-1
40. van Mameren J, Gross P, Farge G, Hooijman P, Modesti M, Falkenberg M, Wuite GJ, Peterman EJ (2009) Unraveling the structure of DNA during overstretching by using multicolor, single-molecule fluorescence imaging. Proc Natl Acad Sci USA 106:18231
41. Veigel C, Bartoo ML, White DC, Sparrow JC, Molloy JE (1998) The stiffness of rabbit skeletal actomyosin cross-bridges determined with an optical tweezers transducer. Biophys J 75:1424
42. Visscher K, Schnitzer MJ, Block SM (1999) Single kinesin molecules studied with a molecular force clamp. Nature 400:184
43. Wang MD, Yin H, Landick R, Gelles J, Block SM (1997) Stretching DNA with optical tweezers. Biophys J 72:1335
44. Wenner JR, Williams MC, Rouzina I, Bloomfield VA (2002) Salt dependence of the elasticity and overstretching transition of single DNA molecules. Biophys J 82:3160
45. Whitelam S, Pronk S, Geissler PL (2008) There and (slowly) back again: entropy-driven hysteresis in a model of DNA overstretching. Biophys J 94:2452
46. Williams MC, Wenner JR, Rouzina I, Bloomfield VA (2001) Effect of pH on the overstretching transition of double-stranded DNA: evidence of force-induced DNA melting. Biophys J 80:874
47. Williams MC, Wenner JR, Rouzina I, Bloomfield VA (2001) Entropy and heat capacity of DNA melting from temperature dependence of single molecule stretching. Biophys J 80:1932
48. Yin H, Wang MD, Svoboda K, Landick R, Block SM, Gelles J (1995) Transcription against an applied force. Science 270:1653